Magic-Angle-Pulse Driven Separation of Degenerate ^{1}H Transitions in Methyl Groups of Proteins: Application to Studies of Methyl Axis Dynamics

Vitali Tugarinov,*[a] Theodoros K. Karamanos,[a] and G. Marius Clore*[a]

Dynamics of protein side chains is one of the principal determinants of conformational entropy in protein structures and molecular recognition events. We describe NMR experiments that rely on the use of magic-angle pulses for efficient isolation of degenerate ^{1}H transitions of the $I=3/2$ manifold of $^{13}CH_3$ methyl groups, and serve as 'building blocks' for the measurement of transverse spin relaxation rates of the fast- and slow-relaxing ^{1}H transitions – the primary quantitative reporters of methyl axis dynamics in selectively {$^{13}CH_3$}-methyl-labelled, highly deuterated proteins. The magic-angle-pulse driven experiments are technically simpler and, in the absence of relaxation, predicted to be 2.3-fold more sensitive than previously developed analogous schemes. Validation of the methodology on a sample of {$^{13}CH_3$}-labeled ubiquitin demonstrates quantitative agreement between order parameters of methyl three-fold symmetry axis obtained with magic-angle-pulse driven experiments and other established NMR techniques, paving the way for studies of methyl axis dynamics in human DNAJB6b chaperone, a protein that undergoes exchange with high-molecular-weight oligomeric species.

Dynamics of protein side chains is one of the principal components of molecular recognition events,[1,2] as well as conformational entropy of protein structures.[3,4] As unique probes of molecular motions, methyl groups play a special role in NMR studies of side-chain dynamics in proteins, providing important insights into a variety of biochemical processes.[5] At the same time, the complexity of the $^{13}CH_3$ methyl spin-system with its multiple degenerate ^{1}H transitions, continues to present a challenge for NMR researchers. Several NMR experiments that address the problem of separation of individual degenerate ^{1}H transitions or their combinations in selectively {$^{13}CH_3$}-methyl-labeled and otherwise deuterated proteins, have been developed.[6–10] One class of experiments aims at quantitative characterization of the motions of the methyl three-fold symmetry axis utilizing the differences between transverse spin relaxation rates of the fast-($R^F_{2,H}$) and slow-($R^S_{2,H}$)-relaxing methyl ^{1}H transitions.[6] These differences are quantitatively related to order parameters of the methyl three-fold symmetry axis, S^2_{axis}, the principal reporter on the amplitudes of methyl axis dynamics. The advantages of using magic-angle pulses or delays tuned for magic-angle dephasing in NMR polarization transfer schemes were realized long ago,[11] and utilized for the measurement of ^{13}C R_1 and R_2 relaxation rates in methyl groups of proteins by Palmer et al.[12] and Kay, Torchia and co-workers.[13,14]

Figure 1 shows the energy level diagram of a spin system consisting of three magnetically equivalent nuclei in a methyl group (H_3). The energy level diagram contains one manifold with spin $I=3/2$ and two with $I=1/2$. All five ^{1}H transitions in Figure 1 are completely degenerate and give rise to a single peak in a NMR spectrum. In the macromolecular limit, transverse spin relaxation of the inner ^{1}H transitions of the $I=3/2$ manifold that is the main focus of the present work, occurs with slower rates ($R^S_{2,H}$, shown with red arrows in Figure 1), whereas the outer ^{1}H transitions of the $I=3/2$ manifold ($R^F_{2,H}$, blue arrows) are characterized by much faster rates of decay.[6]

Recently, we reported optimized NMR schemes for selection of ^{1}H transitions belonging to the $I=1/2$ manifold of a $^{13}CH_3$ methyl group using acute angle RF pulses, thereby achieving significant simplification of the $^{13}CH_3$ spin-system response.[15] Here, we describe NMR experiments for efficient sequestration of degenerate ^{1}H transitions belonging to the $I=3/2$ manifold of the $^{13}CH_3$ methyl group using magic-angle (54.7°) RF pulses. The magic-angle-pulse driven approach is subsequently ex-

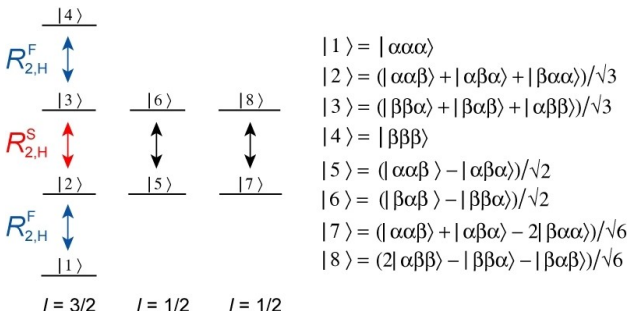

Figure 1. Energy level diagram of the X_3 spin-system of a methyl group. Slow- and fast-relaxing single-quantum ^{1}H transitions of the $I=3/2$ manifold are shown by the red and blue arrows, respectively. The spin quantum numbers, I, of the three manifolds are specified below the diagram. The eight ^{1}H eigenstates described by linear combinations of $|i,j,k>$ ($i,j,k\in\{\alpha,\beta\}$) are shown on the right. The transitions of ^{13}C nuclei have been omitted from the figure for simplicity, although a $^{13}CH_3$ methyl group (AX_3 spin-system) is considered in practice.

[a] Dr. V. Tugarinov, Dr. T. K. Karamanos, Dr. G. M. Clore
Laboratory of Chemical Physics
National Institute of Diabetes and Digestive and Kidney Diseases
National Institutes of Health, Bethesda, Maryland 20892-0520, USA
E-mail: vitali.tugarinov@nih.gov
mariusc@mail.nih.gov

Supporting information for this article is available on the WWW under https://doi.org/10.1002/cphc.202000200

tended to the measurements of $R^F_{2,H}$ and $R^S_{2,H}$ relaxation rates in {$^{13}CH_3$}-methyls of highly deuterated proteins.

In the absence of relaxation, the magic-angle-pulse driven experiments are predicted to be 2.3-fold more sensitive than previously developed schemes.[6,7] The experiments are tested on {U-[^{2}H]; Ileδ1-[$^{13}CH_3$]; Leu,Val-[$^{13}CH_3$,$^{12}CD_3$]}-labeled (ILV-{$^{13}CH_3$}) ubiquitin (8.5 kDa) at 10 and 25 °C. Quantitative agreements between the values of S^2_{axis} obtained with magic-angle-pulse driven separation of ^{1}H coherences and the values derived from earlier ^{2}H relaxation measurements in {$^{13}CH_2D$}-methyl groups[16] or 3Q 'forbidden' spectroscopy,[9] pave the way for application of the methodology to a deletion mutant of the ILV-{$^{13}CH_3$}-labeled human DNAJB6b chaperone, ΔST-DNAJB6b (25 kDa; 25 °C),[17] a challenging system that exchanges between monomeric and high-molecular-weight oligomeric species.

Figures 2A,B show the pulse schemes that have been developed to isolate the coherences belonging to the $I=3/2$ manifold of a $^{13}CH_3$ methyl group. In the experiment of Figure 2A, the application of the $4\tau_b$ element (enclosed in the dashed box) prepares the $^{13}CH_3$ methyl magnetization in a state where only the fast-relaxing coherences (*F*; shown with blue arrows in Figure 1) are present. Subsequent application of a ^{1}H pulse with a flip-angle $\alpha = \cos^{-1}(1/\sqrt{3}) = 54.7°$ (shown in green in Figure 2A) is central to the approach developed here. This pulse converts the fast-relaxing ^{1}H coherences to the slow-relaxing ones of the $I=3/2$ manifold and creates some ^{1}H triple-quantum (*TQ*) coherences, as shown schematically at the top of Figure 2C. Since the rest of the experiment is based on the HMQC 'read-out' scheme, the term containing ^{1}H *TQ* coherences will not lead to observable magnetization at the end of the experiment. Thus, an efficient selection of the inner transitions of the $I=3/2$ manifold is achieved with a loss of only $(1-\sqrt{3}/2)$ ~13 % of their initial intensities.

In the experiment of Figure 2B, the magic-angle ^{1}H pulse (shown in green) is applied immediately after the $2\tau_a$ dephasing period without prior selection for either fast- or slow-relaxing parts of the methyl ^{1}H magnetization. The fast-relaxing (outer) transitions *F* behave under the effect of this pulse in the same manner as in the scheme of Figure 2A (as shown at the top of Figure 2C). The slow-relaxing part of ^{1}H magnetization (*S*) is transformed by the magic-angle pulse as shown schematically in the lower part of Figure 2C, creating some ^{1}H *TQ* coherences, the fast-relaxing coherences *F*, and the slow-relaxing coherences of the $I=3/2$ ($S^{3/2}$) and $I=1/2$ ($S^{1/2}$) manifolds. The latter two, however, have opposite signs (the bottom row in Figure 2C) and cancel each other out during the t_1 and t_2 acquisition periods, as the expectation value of the sum of $S^{1/2}$ and $S^{3/2}$ operators, $(\sqrt{3}/3)S^{1/2}$ - $(\sqrt{3}/6)S^{3/2}$, is zero at the end of the experiment. The fast-relaxing coherences *F* created by the magic-angle pulse are eliminated by the subsequent element $2\tau_b$ in Figure 2B, while ^{1}H *TQ* coherences originating from *F* and *S* (Figure 2C) cancel out, with the remaining observable magnetization consisting solely of the term $S^{3/2}$ corresponding to the inner transitions of the $I=3/2$ manifold that originate from the fast-relaxing (outer) transitions *F*. In the absence of relaxation, the efficiency of this selection is the same as for the scheme in Figure 2A. The scheme in Figure 2B, however, is more relaxation-tolerant than that of Figure 2A, since relaxation decay with the rate of fast-relaxing ^{1}H coherences ($R^F_{2,H}$) occurs for an additional period of duration $4\tau_b$ in the latter. More detailed, quantitative description of the schemes in Figures 2A,B using single-transition spin operators is provided in the Supporting Information (SI).

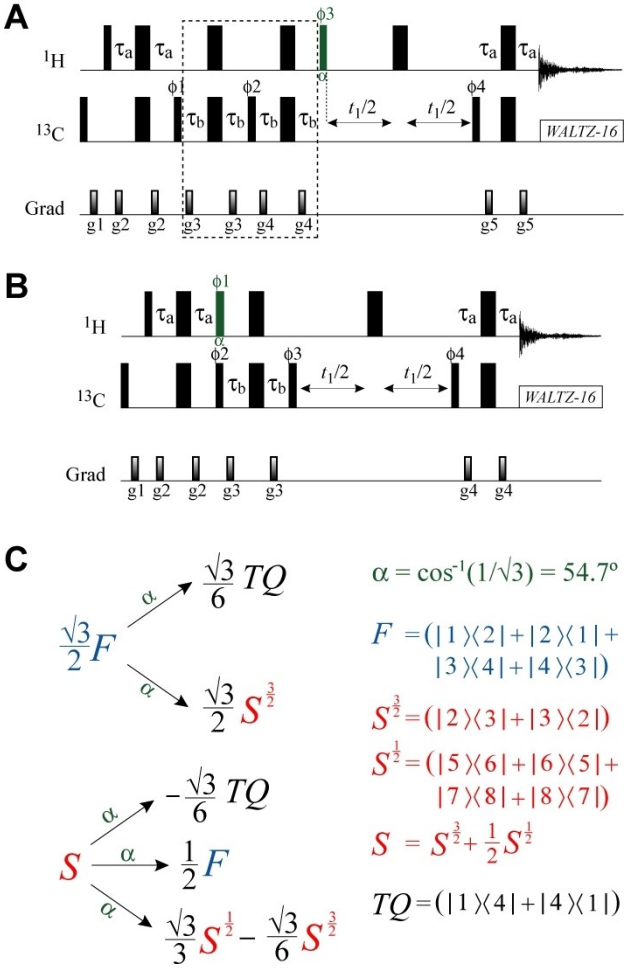

Figure 2. Pulse schemes for separation of inner $I=3/2$ manifold transitions in $^{13}CH_3$ methyl groups with A) selection of fast-relaxing (outer) transitions prior to the magic-angle ^{1}H pulse α (shown in green), and B) cancellation of the inner ^{1}H transitions of the $I=3/2$ manifold and ^{1}H transitions of the $I=1/2$ manifold. Details of experimental parameters are provided in the SI ('Materials and Methods'). C) Schematic diagram describing the transformation of various types of ^{1}H magnetization under the effect of the magic-angle ^{1}H pulse α. Definitions of the ^{1}H fast-relaxing coherences (*F*; blue), the slow-relaxing coherences (*S*; red) and those of the $I=3/2$ and $I=1/2$ keep '1/2' on the same line manifolds ($S^{3/2}$ and $S^{1/2}$; red) are provided in terms of the eight ^{1}H eigenstates (Figure 1) to the right of the diagram.

Using a straightforward extension of the scheme in Figure 2A we verified that the (isolated) inner ^{1}H transitions of the $I=3/2$ manifold ($S^{3/2}$) in {$^{13}CH_3$}-labeled ubiquitin decay with the same transverse relaxation rates as those selected using the phase-cycling based scheme described previously:[7] 8.0 ± 1.2 s^{-1} and 11.2 ± 1.8 s^{-1} at 25 and 10 °C (500 MHz), respectively, measured for the average relaxation rate with the magic-angle-pulse based approach compared to 7.9 ± 1.1 s^{-1} and 11.1 ± 1.7 s^{-1} at 25 and 10 °C, respectively, for the phase-cycling based

experiment.[7] Correlation plots comparing the two sets of relaxation rates obtained for ubiquitin at 25 and 10 °C are provided in the SI, Figure S1. We note that the same verification is not possible for the scheme in Figure 2B since the (selected) ^{1}H magnetization $S^{3/2}$ decays *in the presence* of $S^{1/2}$ and $S^{3/2}$ originating from the slow-relaxing ^{1}H transitions. Although these terms cancel out upon signal observation at the end of the experiment, they can affect each other's rates of decay due to (1) efficient cross-relaxation between the two manifolds in small proteins, or (2) partial 'restoration' of the ^{1}H transitions of the $I=1/2$ manifold ($S^{1/2}$) during the t_1 and t_2 acquisition periods in larger proteins (as $S^{1/2}$ has slower relaxation rates than $S^{3/2}$).[7]

In the absence of relaxation, both schemes in Figures 2A,B recover $\sqrt{3}/2$ of the $S^{3/2}$ magnetization in a single scan. By contrast, the phase-cycling based scheme developed earlier[7] recovers 3/8 of the $S^{3/2}$ magnetization per scan. The predicted improvement in sensitivity ($4/\sqrt{3}=2.31$) agrees well with experimentally obtained average factors of 2.25 and 2.20 for 29 methyls of ubiquitin at 25 and 10 °C (500 MHz), respectively, with the scheme in Figure 2B, and 2.06 and 1.78 at 25 and 10 °C, respectively, with the scheme in Figure 2A. These values are consistent with fast relaxation of methyl signals during the four τ_b periods in the scheme of Figure 2A.

The magic-angle-pulse based separation of degenerate ^{1}H transitions can be applied to the measurement of the fast ($R^F_{2,H}$) and slow ($R^S_{2,H}$) ^{1}H relaxation rates of the outer and inner transitions of the $I=3/2$ manifold in {$^{13}CH_3$}-methyls of highly deuterated proteins. Figure 3A shows such an experiment based on the selection scheme of Figure 2A. The relaxation period T here either precedes (for the measurements of $R^F_{2,H}$) or immediately follows (for the measurements of $R^S_{2,H}$) the magic-angle $^1H_{\phi4}$ pulse (shown with blue or red dashed rectangles for the measurements of $R^F_{2,H}$ and $R^S_{2,H}$, respectively; Figure 3A). In the absence of relaxation, the measurements of $R^F_{2,H}$ in Figure 3A are predicted to be more sensitive than those with the scheme developed earlier[6] by the factor of $4/\sqrt{3}$. However, fast relaxation of the ^{1}H coherences F (in this case during the $2\tau_a$ dephasing period) is expected to 'wipe out' these gains for larger proteins (see SI for more detailed analysis). Nevertheless, the experiment in Figure 3A has the advantage of $R^F_{2,H}$ and $R^S_{2,H}$ being measured with practically the same simple pulse-scheme.

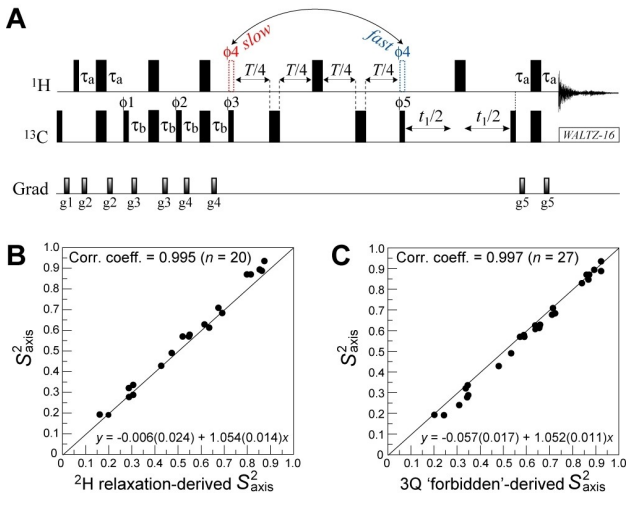

Figure 3. A) Pulse scheme for the measurement of methyl ^{1}H relaxation rates $R^F_{2,H}$ and $R^S_{2,H}$ in $^{13}CH_3$ methyl groups based on the $I=3/2$ transitions selection in the experiment in Figure 2A. Details of experimental parameters are provided in the SI ('Materials and Methods'). Correlation plots comparing the values of S^2_{axis} obtained in ubiquitin at 10 °C ($\tau_C=9$ ns in D_2O) using the experiment in (A) and Eq. (1) (y-axis), and S^2_{axis} derived from ^{2}H relaxation experiments[16] (B) and 3Q-filtered 'forbidden' experiments[9] (C) (x-axis).

The difference between $R^F_{2,H}$ and $R^S_{2,H}$ derives from intra-methyl ^{1}H-^{1}H dipolar cross-correlated relaxation η, and is given by

$$R^F_{2,H} - R^S_{2,H} = 2\eta \approx \frac{9}{5}\left(\frac{\mu_o}{4\pi}\right)^2 \left[P_2\left(\cos\theta_{axis,HH}\right)\right]^2 \frac{S^2_{axis}\gamma_H^4\hbar^2\tau_C}{r^6_{HH}} \quad (1)$$

where τ_C is the global molecular tumbling time (assumed isotropic), μ_0 the vacuum permittivity constant, γ_H the gyromagnetic ratio of a proton spin, r_{HH} the distance between pairs of methyl protons, $\theta_{axis,HH}$ the angle between the methyl three-fold axis and a vector connecting a pair of methyl ^{1}H nuclei, and $P_2(cos\theta)=(1/2)(3cos^2\theta-1)=-1/2$ for ideal tetrahedral methyl geometry. These differences are therefore direct reporters of order parameters of methyl three-fold symmetry axis S^2_{axis}, the principal measure of amplitudes of methyl axis dynamics. The values of S^2_{axis} obtained for methyls of ubiquitin at 10 °C ($\tau_C=$ 9 ns in D_2O) with the scheme in Figure 3A and re-calculated using Equation (1), are compared with S^2_{axis} derived from ^{2}H relaxation measurements[16] in {$^{13}CH_2D$}-methyls and 3Q-filtered 'forbidden' experiments[9] in Figures 3B and 3C, respectively. Very good agreement is obtained between the two sets of S^2_{axis} in both cases despite the fact that ^{1}H coherences $S^{3/2}$ selected in the scheme of Figure 3A, relax (11/9)-fold faster than the coherences F due to dipolar interactions with external ^{1}H spins,[7] slightly compromising the accuracy of Eq. (1) for estimation of S^2_{axis}. Detailed analysis of expected systematic errors in S^2_{axis}, along with the discussion of the effects of dipolar interactions with external protons on the ($R^F_{2,H}$ - $R^S_{2,H}$) differences derived from the experiment in Figure 3A, is provided in the SI (see Figure S2 and associated content).

Analogous experiments for the measurements of $R^F_{2,H}$ and $R^S_{2,H}$ that are based on the scheme in Figure 2B, can be developed (SI, Figure S3A, where the R_2 of $S^{3/2}+(1/2)S^{1/2}$ is measured). Although good agreement is achieved between the sets of S^2_{axis} derived from these experiments and those obtained from ^{2}H relaxation (Figure S3B) or 3Q 'forbidden' experiments (Figure S3C) in ubiquitin at 10 °C, we predict that the scheme in Figure S3A will provide reliable S^2_{axis} values only in a narrow range of correlation times τ_C due to partial 'restoration' of the ^{1}H transitions of the $I=1/2$ manifold ($S^{1/2}$) during the t_1 and t_2 acquisition periods (see SI for a brief discussion of this effect).

Having established the validity of the magic-angle based selection scheme, we turned to the study of methyl axis dynamics in a more challenging system, namely the deletion mutant of the ILV-{$^{13}CH_3$}-labeled human DNAJB6b chaperone, ΔST-DNAJB6b (25 kDa), that undergoes spontaneous oligomerization and has been shown to exchange between the free monomeric state and high-molecular-weight oligomers (~35-40

monomeric units) at concentrations above ~100 μM.[17] The structure of ΔST-DNAJB6b comprises two domains that tumble independently of one another: the well-ordered helical J domain (JD) and a more flexible C-terminal β-sheet domain (CTD), implicated in self-association. The average values of $R^F_{2,H}$ and $R^S_{2,H}$ of 113 ± 7 and 13 ± 1 s^{-1}, respectively, were measured for the JD domain of ΔST-DNAJB6b at a concentration of 200 μM using the scheme in Figure 3A. The corresponding rates for the CTD domain are 47 ± 2 and 8 ± 1 s^{-1}, respectively. From the estimated population of ~2% for the higher-order complex of ΔST-DNAJB6b at a concentration of 200 μM (in monomer units) based on our earlier study,[17] we estimate apparent rotational correlation times τ_C of 24 and 16 ns for the JD and CTD domains, respectively, in D_2O (25 °C) (see SI, 'Materials and Methods'). The set of S^2_{axis} values obtained for ΔST-DNAJB6b is shown in Figure 4A for the JD and CTD domains (Figure 4B). These values of S^2_{axis} are in good agreement with those derived from the 3Q-filtered 'forbidden' spectroscopy (Figure 4C). Relative flexibilities of the JD and CTD domains inferred earlier from backbone amide ^{15}N relaxation data,[17] are clearly borne out by the analysis of methyl axis dynamics. The S^2_{axis} values steadily decrease towards the C-terminus of the protein (Figure 4A), implying that higher conformational entropy of this region is conducive to side-chain interactions implicated in oligomerization of ΔST-DNAJB6b. Of note, Ile140$^{\delta1}$ and Ile176$^{\delta1}$ methyl protons show substantial exchange line-broadening, R_{ex}, due to the inter-conversion between monomeric and high-order oligomeric species.[15] Nevertheless, their S^2_{axis} values are not affected by exchange, as R_{ex} is largely subtracted out in the ($R^F_{2,H}$-$R^S_{2,H}$) difference (see Equation (1)).

In summary, we have shown that the use of magic-angle RF pulses enables efficient selection of degenerate ^1H transitions belonging to the $I = 3/2$ manifold of $^{13}CH_3$ methyl groups. The magic-angle-pulse driven approach is applied to the measurement of transverse relaxation rates of the fast- and slow-relaxing ^1H transitions that serve as quantitative reporters of methyl axis dynamics in selectively {$^{13}CH_3$}-labeled, deuterated proteins. The methodology is validated using {$^{13}CH_3$}-labeled ubiquitin providing quantitative agreements between methyl axis order parameters obtained with the magic-angle-pulse based experiment and other established NMR techniques, and extended to studies of methyl axis dynamics in the human DNAJB6b chaperone that inter-converts between monomeric and high-molecular-weight oligomeric species.

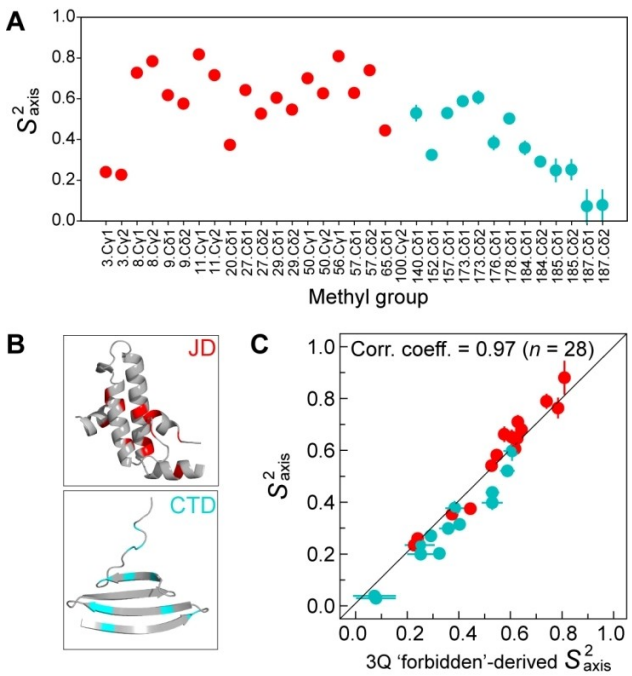

Figure 4. A) S^2_{axis} values obtained for the methyls of {U-[^2H]; Ileδ1-[$^{13}CH_3$]; Leu,Val-[$^{13}CH_3$,$^{12}CD_3$]}-labeled ΔST-DNAJB6b (200 μM; 600 MHz; 25 °C) using the scheme in Figure 3A. The methyl sites of the JD and CTD domains are shown in red and cyan, respectively. See SI 'Materials and Methods' for details of NMR acquisition and analysis. B) Ribbon diagrams of the two domains of ΔST-DNAJB6b, JD and CTD, with positions of the backbone atoms of the analyzed methyl-bearing residues colored in red (JD) and cyan (CTD). C) Correlation plot comparing the values of S^2_{axis} obtained for the methyls of ΔST-DNAJB6b using the experiment in Figure 3A (*y*-axis), and those derived from the 3Q-filtered 'forbidden' experiment[9] (*x*-axis).

Supporting Information

Description of the evolution of magnetization during the pulse-schemes in Figures 2A,B using single-transition spin operators. Figure S1 showing the correlation plots comparing transverse spin relaxation rates of the inner $I = 3/2$ manifold transitions keep '$S^{3/2}$' on the same line ($S^{3/2}$), $R^S_{2,H}$, obtained in ubiquitin using the extension of the scheme in Figure 2A and the phase-cycling approach in ref. [7] at 25 and 10 °C. Figure S2 showing simulated systematic errors in S^2_{axis} expected from the experiment in Figure 3A as a function of the density of external proton spins. A discussion of the effects of dipolar interactions with external protons on the ($R^F_{2,H}$ - $R^S_{2,H}$) differences derived from the experiment in Figure 3A. Figure S3 showing the experiment for the measurement of $R^F_{2,H}$ and $R^S_{2,H}$ that is based on the scheme in Figure 2B, along with the agreement between the sets of S^2_{axis} values derived from this experiment and those obtained from other established NMR techniques in ubiquitin at 10 °C. A discussion of partial restoration of the ^1H transitions of the $I = 1/2$ manifold ($S^{1/2}$) during the t_1 and t_2 acquisition periods of the schemes in Figures 2B and S3A. 'Materials and Methods' section describing the procedures of NMR sample preparation and NMR experimental details.

Acknowledgements

The authors thank Drs. Dan Garrett, Jinfa Ying and James Baber for technical support. This work was supported by the Intramural Program of the National Institute of Diabetes and Digestive and Kidney Diseases, National Institutes of Health (DK029023 to G.M.C.).

Conflict of Interest

The authors declare no conflict of interest.

Keywords: methyl NMR · $^{13}CH_3$ spin-system · side-chain dynamics · methyl axis order parameters · proteins

[1] K. K. Frederick, M. S. Marlow, K. G. Valentine, A. J. Wand, *Nature* **2007**, *448*, 325–329.
[2] R. Sprangers, L. E. Kay, *Nature* **2007**, *445*, 618–622.
[3] M. Akke, R. Bruschweiler, A. Palmer, *J. Am. Chem. Soc.* **1993**, *115*, 9832–9833.
[4] T. I. Igumenova, K. K. Frederick, A. J. Wand, *Chem. Rev.* **2006**, *106*, 1672–1699.
[5] R. Rosenzweig, L. E. Kay, *Annu. Rev. Biochem.* **2014**, *83*, 291–315.
[6] V. Tugarinov, L. E. Kay, *J. Am. Chem. Soc.* **2006**, *128*, 7299–7308.
[7] V. Tugarinov, L. E. Kay, *J. Am. Chem. Soc.* **2007**, *129*, 9514–9521.
[8] V. Tugarinov, R. Sprangers, L. E. Kay, *J. Am. Chem. Soc.* **2007**, *129*, 1743–1750.
[9] H. Sun, L. E. Kay, V. Tugarinov, *J. Phys. Chem. B* **2011**, *115*, 14878–14884.
[10] K. Pervushin, B. Vogeli, *J. Am. Chem. Soc.* **2003**, *125*, 9566–9567.
[11] O. W. Sorensen, R. R. Ernst, *J. Magn. Reson.* **1983**, *51*, 477–489.
[12] A. G. Palmer, P. E. Wright, M. Rance, *Chem. Phys. Lett.* **1991**, *185*, 41–46.
[13] L. E. Kay, T. E. Bull, L. K. Nicholson, C. Griesinger, H. Schwalbe, A. Bax, D. A. Torchia, *J. Magn. Reson.* **1992**, *100*, 538–558.
[14] L. K. Nicholson, L. E. Kay, D. M. Baldisseri, J. Arango, P. E. Young, A. Bax, D. A. Torchia, *Biochemistry* **1992**, *31*, 5253–5263.
[15] V. Tugarinov, T. K. Karamanos, A. Ceccon, G. M. Clore, *ChemPhysChem* **2020**, *21*, 13–19.
[16] X. Liao, D. Long, D. W. Li, R. Bruschweiler, V. Tugarinov, *J. Phys. Chem. B* **2012**, *116*, 606–620.
[17] T. K. Karamanos, V. Tugarinov, G. M. Clore, *Proc. Natl. Acad. Sci. USA* **2019**, *116*, 21529–21538.

Manuscript received: March 12, 2020
Revised manuscript received: April 3, 2020
Accepted manuscript online: April 3, 2020
Version of record online: April 29, 2020